Surface and interfacial creases in a bilayer tubular soft tissue

Mir Jalil Razavi, Ramana Pidaparti, and Xianqiao Wang

Phys. Rev. E **94**, 022405 — Published 9 August 2016

DOI: 10.1103/PhysRevE.94.022405

Surface and interfacial creases in a bilayer tubular soft tissue

Mir Jalil Razavi, Ramana Pidaparti, and Xianqiao Wang*

College of Engineering, University of Georgia, Athens, GA 30602

Corresponding author email: xqwang@uga.edu

Surface and interfacial creases induced by biological growth are common types of instability in soft biological tissues. This study focuses on the criteria for the onset of surface and interfacial creases as well as its morphological evolution in a growing bilayer soft tube within a confined environment. Critical growth ratios for triggering surface and interfacial creases are investigated both analytically and numerically. Analytical interpretations provide preliminary insights into critical stretches and growth ratios for the onset of instability and formation of both surface and interfacial creases. However, the analytical approach cannot predict the evolution pattern of the model after instability, therefore non-linear finite element simulations are carried out to replicate the post-stability morphological patterns of the structure. Analytical and computational simulation results demonstrate that the initial geometry, growth ratio, and shear modulus ratio of the layers are the most influential factors to control surface and interfacial crease formation in this soft tubular bilayer. The competition between the stretch ratios in the free and interfacial surfaces is one of the key driving factors to determine the location of the first crease initiation. These findings may provide some fundamental understanding in the growth modeling of tubular biological tissues such as esophagi and airways as well as offering useful clues into normal and pathological functions of these tissues.

Keywords: Surface crease, Interfacial crease, Biological growth, Finite element analysis

1. Introduction

Growth and remodeling of a developing soft biological tissue are two highly complex processes which have crucial effects in the normal development and pathological status of a biological tissue [1]. It has been shown that mechanical factors have considerable influence on the growth and remodeling of growing structures beside the biological and genetic factors [1-4]. Generally, biological tissues are composed of multiple layers of different thicknesses, material properties, and growth rates; e.g. the skin [5], brain [6], artery [7], gut [8], and esophagus [9]. Non-uniform growth results in the appearance of strain mismatch among the layers and leads to the advent of residual stresses [10]. This stress is created due to the integrity of the biological structures preventing self-overlap or overlap between tissues [11-14]. Residual stress is also believed to play a crucial role in morphogenesis and regulation of the material properties of biological systems [12,15-17]. It has been proven that once the compressive residual stress exceeds a critical value, in order to release its potential energy the tissue buckles into a new configuration [12]. Beyond the critical condition, three common types of morphological instability can be observed: wrinkling, folding, and creasing [1]. In contrast to wrinkling and folding phenomena, creasing in soft biological tissues (especially the interfacial creasing) has not been well studied and addressed appropriately. Therefore, it is necessary to find a systematic approach to analytically and numerically quantify crease formation in the soft biological tissues.

Creases with sharp edges usually form in soft materials without a hard skin when beyond a certain critical value of compression, depending on material properties [18-21]. One of the main characteristics of creases is the development of self-contact phenomenon after instability. Creases bifurcate locally in space and are large in amplitude, in contrast to wrinkles which bifurcate non-locally in space and are comparatively minuscule in amplitude. Studies show that a flat and soft slab, after having a critical compressive strain applied, starts to develop creases, and the anisotropy of applied strains controls the pattern of creases [22]. Critical strain for the onset of surface creases in a single layer is lower than that for the onset of surface wrinkles [23]. However, it should be mentioned that, for a bilayer structure with comparable elastic moduli for both layers, the critical strain required for the onset of creases can be either smaller or larger than that for the onset of wrinkles. It depends on ratios of the moduli and thicknesses

of both layers [24]. It has been shown that during growth, multilayer hyperelastic soft tissues with considerable differences in the shear moduli of each layer tend to develop wrinkles [1,9], while the same structures using layers with material properties more similar to each other prefer to develop creases [25-27]. Beyond the simple sinusoidal wrinkling, new complex morphologies emerge in a multilayer structure being compressed or grown, e.g. period-doubling and period- quadrupling [9]. Recent study showed that this kind of instability can be also observed in a low stiffness regime and that pattern formation is highly sensitive to small imperfections [28]. It is worthwhile to mention that classical linear perturbation analysis is able to predict the critical condition for the onset of wrinkles, whereas it fails to determine the critical condition for the onset of creases [29]. Generally, creases may be divided into two types: surface creases and interfacial creases. Although the formation mechanisms of both kinds of creases are almost the same, there are still a few differences between the critical strain and shape selection [30]. A surface with a neo-Hookean incompressible material under compression can generate creases on its free surface when the stretch ratio (normal to the tangential) reaches a critical amount; and this critical value does not depend on the shear modulus of the material [29]. But for the onset of an interfacial crease between two bonded neo-Hookean materials, the critical compressive strain depends on the shear modulus ratio of the two layers [30]. In a surface crease, the material develops a self-contact pattern, but in an interfacial crease the presence of two materials prevents the interface from self-contact, so this kind of crease is V-shaped [30]. A recent experimental study has shown that interfacial creases always form at a lower compression than interfacial wrinkles do [30]. Fig. 1 shows mucosal wrinkling of a bovine esophagus. Since the mucosa is much stiffer than the submucosa, the mucosa forms a wrinkled pattern on the submucosa. Interfacial creases also can be detected in the interface between the submucosa and muscle which has been not addressed before. Indeed, it is worth exploring the mechanism and shape selection of interfacial creases in soft tissues.

Few types of research have been done related to surface creases, especially in the case of interfacial creases in the biological tissues, whereas wrinkling and folding phenomena in growing multilayer biological tissues have been studied widely [31-35]. The main goal of this study is to

develop a computational mechanical model to seek answers to what factors contribute to the formation of surface and interfacial creases in a developing bilayer biological tissue. In what follows, we also strive to answer these two intriguing questions: how do contributing factors control the priority of the structure morphology to produce surface or interfacial creases and why are surface creases more common than interfacial creases in biological tissues? In order to answer these, we will construct plane-strain tubular bilayer structures with varying thicknesses, growth ratios, and material properties. Both theoretical and computational approaches will be utilized to determine deformation and stress fields of the growing structure and present the surface morphology after instability. Findings from this study are applicable to interpret the interfacial creases in the tubular multilayer organs like esophagi or invagination of a soft tissue in an elastic environment and the creation of villi in the gut of various species [8].

2. Methods

A. Theoretical method

Due to biological growth, the final state of the tissue system is different from the initial one. Theoretical models have attempted to relate this type of growth to the deformation and stress fields [13]. Any point $\boldsymbol{X}$ in the reference state will be mapped by transformation to the point $\boldsymbol{x}$ in the current state. For modeling volumetric growth we consider the most popular theory, namely, multiplicative decomposition of the deformation gradient [14]. In this theory the deformation gradient, $\boldsymbol{F}(\boldsymbol{X})$, is decomposed into a growth tensor $\boldsymbol{G}(\boldsymbol{X})$ indicating the addition of materials and an elastic deformation tensor $\boldsymbol{A}(\boldsymbol{X})$ describing pure deformation resulting from stress, as shown in Fig. 2. The growth tensor maps the stress-free, ungrown reference configuration to a grown stress-free state, then the elastic deformation tensor maps the grown and unstressed state to a stressed and final current state [14]. The deformation gradient $\boldsymbol{F}$ maps the tissue from a stress-free state before growth to a stressed state after growth.

$$\boldsymbol{F} = \boldsymbol{A}.\boldsymbol{G} \tag{1}$$

where $\boldsymbol{F} = \partial \boldsymbol{x}/\partial \boldsymbol{X}$. While both $\boldsymbol{G}$ and $\boldsymbol{A}$ tensors may be incompatible deformations, their multiplication, $\boldsymbol{F}$, should be a compatible deformation [14]. In general, the elastic deformation of living soft tissues yields little volume change; therefore, the nonlinear response of these

materials can be described by an isotropic incompressible hyperelastic material. The incompressibility implies the determinant of the elastic deformation tensor should be equal to unit, i.e. $det\boldsymbol{A} = 1$. In general, the growth tensor depends on the stress state, deformation, and some other factors. For simplicity, we assume the growth process with a known spatial distribution, insinuating that all the biological information is independent of stresses [12].

Many biological soft tissues can be modeled by a hyperelastic material with a strain energy function $W(\boldsymbol{A})$. The Cauchy stress $\boldsymbol{\sigma}$ is related to the strain energy function by [12]

$$\boldsymbol{\sigma} = \boldsymbol{A}\frac{\partial W}{\partial \boldsymbol{A}} - p\boldsymbol{I} \tag{2}$$

where p is the Lagrangian multiplier to ensure incompressibility condition and $\boldsymbol{I}$ is a second-order unit vector. In the absence of any body force, mechanical equilibrium imposes

$$\mathrm{div}\,\boldsymbol{\sigma} = 0 \tag{3}$$

where "div" stands for the divergence operator in the current configuration. There are several proposed material behaviors for hyperelastic materials [36]; here a simple and common model, isotropic nonlinear Neo-Hookean, is implemented.

$$W = \frac{\mu}{2}({\lambda_r}^2 + {\lambda_\theta}^2 + {\lambda_z}^2 - 3) \tag{4}$$

where μ is the shear modulus and λ_r, λ and λ_z are the radial, circumferential and axial principal stretches, respectively.

Consider a tubular soft bilayer with layers of different material properties growing within a rigid confinement. The outer layer of the tissue is considered to be fixed as shown in Fig. 2. This ideal assumption is considered to mimic the confining effect of a surrounding environment. The inside and outside radii of the inner layer are A and B, and the inside and outside radii of the outer layer are B and C. The initial and undeformed configuration for the tube is defined by $\boldsymbol{X} = (R, \Theta, Z)$

$$A \le R \le C, \qquad 0 \le \Theta \le 2\pi, \qquad 0 \le Z \le L, \tag{5}$$

where R, Θ and Z are cylindrical coordinates in the reference state. L is the longitudinal length of the tube. B is the interface radius between the two bonded layers. Due to the biological growth, the tube deforms axisymmetrically before the occurrence of instability. Growth may

occur in the inner layer, outer layer or both of them. The new and current configuration after growth is defined by $\boldsymbol{x} = (r, \theta, l)$

$$a \leq r \leq c, \qquad 0 \leq \theta \leq 2\pi, \qquad 0 \leq z \leq l, \tag{6}$$

where r, θ and z are cylindrical coordinates in the deformed state and l is the deformed axial length of the tube. b is the interface radius after the growth and deformation. In the case of axisymmetric and plane-strain deformation, the deformation field after growth is just a function of the radius, $r = r(R)$. So, the circumferential and longitudinal coordinates in both undeformed and deformed states keep the same.

For isotropic growth, the growth tensor can be characterized by $\boldsymbol{G} = g\boldsymbol{I}$, where g 1 is for growth, $0g1$ represents atrophy, and $\boldsymbol{I}$ is the unit tensor. But by the assumption of plane-strain conditions without deformation or growth in the axial direction, g_z is considered to be unit.

B. Numerical method

A layered computational model based on the non-linear finite element method with isotropic growth is implemented to capture realistic morphologies of a biological structure after the onset of instability. The model of both the inner and outer layers is considered to be a neo-Hookean hyperelastic material, and growth is simulated via thermal expansion [18,37]. The free surface of the inner layer is allowed to self-contact. The fixed boundary condition is applied in the outer radius of the outer layer. Dynamic-Explicit solver in the commercial software ABAQUS (version6.13), which is suitable for large deformation, nonlinear, and quasi-static problems is implemented to depict patterns changes in the model. Both layers mesh with the plane-strain elements where different mesh sizes are used to ensure the robustness of the simulation results and mesh independence. Following the incompressibility we used in this biological structure, the growth ratio of the layer (g_i) can be defined as the square root of the ratio of the deformed surface area S_i to the initial surface area S_{0_i}, $g_i^2 = S_i/S_{0_i}$, where $i = 1$ represents the inner layer and $i = 2$ the outer layer.

3. Results and Discussions

A. Deformation field and residual stress

By applying the deformation gradient in a cylindrical coordinate for the presented model in Fig. 2 and from Eq. (1), the elastic deformation tensor can be extracted

$$\boldsymbol{A} = diag(\lambda_r, \lambda_\theta, \lambda_z) \qquad \lambda_r = \frac{g^{-1}\partial r}{\partial R}, \qquad \lambda_\theta = \frac{g^{-1} r}{R}, \;\; \lambda_z = 1 \tag{7}$$

which λ_i is the principal stretch. With the incompressibility constraint $det\boldsymbol{A} = 1$, we have

$$\frac{r}{R}\frac{\partial r}{\partial R} = g^2 \tag{8}$$

Integration of Eq. (8) on the boundary of two layers with imposed boundary conditions gives the deformation field of the structure

$$r^2 - a^2 = {g_1}^2(R^2 - A^2) \qquad \text{for} \quad A \le R \le B \tag{9}$$

$$r^2 - C^2 = {g_2}^2(R^2 - C^2) \qquad \text{for} \quad B \le R \le C \tag{10}$$

which $g_1$and g_2 are isotropic growth ratios for the inner layer and outer layer, respectively. Boundary conditions are fixed boundary in the C and continuity in the interfacial radius between two layers ($R = B$). By continuation in the interface, the deformed inner radius a of the structure is

$$a = \left[C^2 - {g_2}^2(C^2 - B^2) - {g_1}^2(B^2 - A^2)\right]^{1/2} \tag{11}$$

and the deformed interface radius b is

$$b = \left[C^2(1 - {g_2}^2) + {g_2}^2 B^2\right]^{1/2} \tag{12}$$

Eqs. (9-12) describe the deformation of the tubular structure induced by growth. For preventing self-contact at the inner radius of the structure after growth, the isotropic growth ratios should satisfy $a > 0$.

Stretch ratios have been demonstrated as a determining factor to trigger instability in soft materials [18,29]. For the sake of further implementation, it is necessary here to detail their derivations. Let $\lambda = \lambda_\theta$, the assumption $det\boldsymbol{A} = 1$ leads to $\lambda_r = \lambda^{-1}$. Based on Eqs. (7, 9, 10, and 11), λ in both layers can be derived

$$\lambda_1 = [1 - (A/R)^2 + (a/g_1 R)^2]^{1/2} \qquad A \le R \le B \tag{13}$$

$$\lambda_2 = [1 - (C/R)^2 + (C/g_2 R)^2]^{1/2} \qquad B \le R \le C \tag{14}$$

where the subscript 1 is for the inner layer and 2 for the outer layer. λ_2 is just a function of the growth ratio in the outer layer, whereas λ_1 is a function of both growth ratios in the inner and outer layers. Based on Eqs. (2) and (4) the Cauchy stress components are derived as

$$\sigma_{rr} = \mu\lambda^{-2} - p, \qquad \sigma_{\theta\theta} = \mu\lambda^2 - p \tag{15}$$

The equilibrium equation, Eq. (3), is derived as

$$\frac{\partial \sigma_{rr}}{\partial r} + \frac{\sigma_{rr} - \sigma_{\theta\theta}}{r} = 0 \tag{16}$$

After derivations, with Eqs. (13-16) the stress distribution can be expressed for the inner layer as

$$\sigma_{rr_1} = \frac{\mu_1}{2}\left[{\lambda_1}^{-2} - {\lambda_{a1}}^{-2} + ln({\lambda_{a1}}^2/{\lambda_1}^2)\right] \qquad A \le R \le B \tag{17}$$

$$\sigma_{\theta\theta_1} = \sigma_{rr_1} + \mu_1({\lambda_1}^2 - {\lambda_1}^{-2}) \qquad A \le R \le B \tag{18}$$

where μ_1 is the shear modulus of the inner layer and $\lambda_{a1} = a/g_1 A$. Using the same approach for the outer layer gives

$$\sigma_{rr_2} = \sigma_{rr_1}\big|_{\lambda_1 = \lambda_{b1}} + \frac{\mu_2}{2}\left[{\lambda_2}^{-2} - {\lambda_{b2}}^{-2} + ln({\lambda_{b2}}^2/{\lambda_2}^2)\right] \quad \text{for} \quad B \le R \le C \tag{19}$$

$$\sigma_{\theta\theta_2} = \sigma_{rr_2} + \mu_2({\lambda_2}^2 - {\lambda_2}^{-2}) \qquad \text{for } B \le R \le C \tag{20}$$

where μ_2 is the shear modulus of the outer layer, $\lambda_{b1} = b/g_1 B$, and $\lambda_{b2} = b/g_2 B$.

The thickness of layers is variable so as to be able to parametrically capture thickness effects on the growth, instability, and remodeling of the tubular bilayer. For a special case, $A = 1$, $B = 1.2$ and $C = 2$, Fig. 3 shows the deformation field and stretches (λ) for a growing bilayer structure with two different growth cases.

For the sake of simplicity, results are mapped to the initial configuration of the structure. As can be noticed from Fig. 3, the deformation field between the inner and outer layers is continuous as expected, but stretches at the interface are not continuous and have jumps. The higher

growth ratio in the outer layer leads to more deformation and higher stretches in both layers. It is also noteworthy to mention that stretch is not a function of the material properties of the layers but rather a function of its geometry and growth.

Fig. 4 illustrates that in the absence of external loads, growth induces residual stresses in both layers. Representative parameters are $\mu_2/\,\mu_1 = 10,\ A = 1,\ B = 1.2,\ C = 2,\ g_1 = 1,$ and $g_2 = 1.05$. Cauchy radial and circumferential stresses are normalized by the modulus ratio of the inner layer; $\bar{\sigma}_{rr} = \sigma_{rr}/\,\mu_1$ and $\bar{\sigma}_{\theta\theta} = \sigma_{\theta\theta}/\,\mu_1$.

Due to the biological growth, the maximum circumferential stress occurs on the free surface of the inner layer [19]. Compressive circumferential stress is observed to be discontinuous at the interface with a lower magnitude in contrast to the stress at the free surface. Several previous studies have revealed that beyond a critical point, compressive stresses in the free surface or interface of soft materials may lead to the formation of creases [18,25,26,29,30,38]. These compressive stresses may play an important role in the instability and shape evolution of the model.

B. Stretch ratio and instability

In order to find the critical strain for the onset of surface or interfacial creases in an incompressible neo-Hookean material, creasing instability has been analyzed by comparing the elastic energy in a creased elastomer and that in a smooth elastomer [29,30]. Results of these studies show that the critical strain for onset of creases on the free surface is $\varepsilon_c \approx 0.35$ and for the interfacial creases it is a function of the modulus ratio of the layers. In both surface and interfacial creases, critical strains are independent of any length scale. In fact, the surface crease is a special case of interfacial crease in which the modulus ratio of the stiff layer to the soft layer is infinite. The critical strain for the onset of interfacial creasing decreases as the modulus ratio of the stiff layer to the soft layer increases [30]. Calculation has shown that when an incompressible neo-Hookean material in the plane-strain condition is compressed to a critical point, the normal to tangential stretch ratio is close to 2.4 [29] equivalent to the critical strain $\varepsilon_c \approx 0.35$. This beneficial number has been used in several studies to predict critical growth ratios for the onset of surface creases in growing structures [18,19,39]. However, the

mechanism and criteria for the onset of surface and interfacial creases in biological tissues have not been addressed very well. In what follows, we are going to unravel these issues.

Following the idea of the critical stretch ratio, in our model for the onset of surface creases in the inner layer, the radial to circumferential stretch ratio should satisfy $\lambda_r/\lambda_\theta \geq 2.4$. But for the onset of interfacial creases between the inner and outer layer this critical stretch ratio is assumed to be a function of their modulus ratio, i.e. $\lambda_r/\lambda_\theta = f(\mu_2/\mu_1)$. Fig. 5 shows the dependency of the critical stretch ratio ($\lambda_r/\lambda_\theta|_{critical}$) on the shear modulus ratio of the two bonded layers for the onset of interfacial creases which it has been derived from Ref [30]. Here we will focus on models with a higher shear modulus in the outer layer than in the inner layer. If the inner layer of a structure has a higher shear modulus ratio than the outer layer, it will typically generate wrinkles in a stiff layer on a soft substrate; a phenomenon which has been well reported in many literatures [31,34,40,41].

Fig. 5 shows that the critical stretch ratio for the onset of interfacial creases decreases as the modulus ratio of the bilayer increases. In the limiting case $\mu_2/\mu_1 = \infty$, the critical stretch ratio approaches to the critical one in surface creases, $\lambda_r/\lambda_\theta \approx 2.4$. When the shear modulus ratio is close to unit, two layers can be considered as a uniform hyperelastic material in which it is difficult to initiate the interfacial crease even in high compressive strains, $_c \approx 1$. The presence of the surface creases on the inner layer or interfacial creases depends on the competition of the critical stretch ratio (λ_r/λ_θ) between the inner surface and the interface of the bilayer structure. With the definition $\lambda = \lambda_\theta$ and $\lambda = {\lambda_r}^{-1}$ the radial to circumferential stretch ratio is $\lambda_r/\lambda_\theta = 1/\lambda^2$ where λ for both inner and outer layers have been derived in Eqs. (13) and (14). Fig. 6 depicts the radial and circumferential stretches and their ratio in a growing structure with $A = 1$, $B = 1.2$, $C = 2$, and $g_2 = 1.05$. The competition between the stretch ratios in the free and interfacial surfaces is one of the key driving factors to determine the location of the first crease initiation. The modulus ratio between two layers also plays an important role in the determination of the crease formation. By comparing the data from Fig. 6 with the critical values from Fig. 5, we can find the critical growth ratios for specific cases to start instability and crease formation as well as the location of crease formation.

Eqs. (13) and (14) imply that the initial interfacial geometry in each layer can affect the stretch ratio during the deformation. Fig. 7 shows the dependency of the stretch ratio for each layer on their geometry with the structural parameters $A = 1$ and $C = 2$ as well as the growth ratios $g_1 = 1$ and $g_2 = 1.1$. There are two different cases: one with the interface at $B = 1.5$ and the other one at $B = 1.8$.

From Fig. 7, it can be noticed that as the position of the interface changes, the stretch ratio respond accordingly in both layers. A higher thickness of the outer layer leads to more deformation and higher stretch ratio of the structure under biological growth. Also, it is interesting to see that the maximum stretch ratio may occur either on the free surface or the interface.

In order to clearly find the maximum stretch ratio in the structure, Fig. 8 depicts the maximum stretch ratio in the free and the interfacial surfaces under different interface radii with the growth ratio $g_2 = 1.1$ in the outer layer. From Fig. 8, there is a competition of the maximum stretch ratio between the free surface and the interface of the structure. By comparing each maximum stretch ratio with the corresponding critical one for the onset of surface or interfacial creases, the position of the first crease can be determined. For a lower thickness of the inner layer ($B \leq 1.7$ for this case), the maximum stretch ratio occurs in the free surface while for a higher thickness of the inner layer ($B \geq 1.7$) the maximum stretch ratio occurs in the outer layer. In addition to the interface radius, growth ratios g_1 in the inner layer and g_2 in the outer layer may have crucial effects on the stretch ratio in the free and interfacial surfaces. Fig. 9 shows three cases with different growth ratios in the structure: (a) growth in the inner layer, (b) growth in the outer layer, and (c) growth in both layers. These three cases are able to cover all possibilities in the formation of surface, interfacial, or both types of creases.

Fig. 9(a) clearly states that if growth just occurs in the inner layer of the structure, there are no stretches in the outer layer. This result shows that growth in the inner layer only has the potential to create surface creases but not interfacial creases. The higher the growth ratio of the inner layer, the higher the stretch ratio the free surface experiences. Fig. 9(b) illustrates

that if growth just takes place in the outer layer, a significant stretch ratio can be observed even on the free surface of the inner layer. Therefore, it is expected that by the growth of the outer layer, surface creases can be produced on the free surface. Moreover, the interface may also experience a considerable stretch ratio which can lead to the formation of interfacial creases. Fig. 9(c) shows an example of the case which growth takes place in both layers, wherein high stretch ratio can be observed in both free and interfacial surfaces. The dotted line in Fig.9(c) indicates that both the inner and outer layers have the same growth ratio which makes the stretch ratio continuous across the interface. The behaviors of the third case in Fig. 9(c) can roughly be mimicked by the second case through considering more growth in the outer layer. Also, the second case can cover both surface and interfacial creases which just depend on a single variable, the growth ratio in the outer layer, g_2. Therefore, for simplicity we would like to focus on the model based on the second case from Fig. 9(b) to investigate the critical growth ratio and the morphological evolution after instability in the following sections.

C. Crease formation and critical growth ratio

It was found that the stretch ratio and the material properties of the layers are determining factors to initiate surface and interfacial creases in a soft tubular bilayer. The maximum value of the stretch ratio in the free or the interfacial surface is determined by the initial geometry and growth ratio of the bilayer structure. It is not easy to calculate the growth ratio of layers *in vivo,* therefore we dynamically increase the growth ratio from a unit to the value where the system initiates instability and creasing. Pathological disorders affect the growth ratio and overgrowth of layers may lead to obstruction in organs such as airways and esophagi [9,32,33].

Here we want to show how surface and interfacial creases are developed step by step through a special case. Fig. 10 shows the dependency of the stretch ratio ($\lambda_r / \lambda_\theta$) at the free surface and interface on the growth ratio of the outer layer. For this case the interface radius is $B = 1.2$ and both free surface and interface stretches are unity at the starting point of growth. When the bilayer structure starts to grow, the stretch ratios at both the free and interfacial surface increase while the stretch ratio in the free surface grows faster than that in the interface. When the stretch ratio of the free surface reaches 2.4, creases start to form on the free surface of the inner layer. At this point, the maximum stretch ratio at the interface has not reached the critical

point yet, therefore the interface does not experience any interfacial creases. However, as the growth continues we can eventually observe the onset of creases in the interface when the critical stretches ratio of the interface reaches $\lambda_r/\lambda_\theta|_{crit} = 3.23$. Since the critical interfacial stretch ratio is a function of the shear modulus ratio of the bilayer as shown in Fig. 5, a lower shear modulus ratio of the bilayer structure leads to a higher growth ratio needed for the onset of interfacial creasing.

It is very interesting to relate the initiation of creases with the critical growth ratio of the structure, which can provide insights into the growth and dynamic morphological changes of the structure. Following Eqs. (13) and (14), the critical growth ratio for the onset of surface and interfacial creases can be derived based on the initial geometry of the structure. The stretch ratio (λ_r/λ_θ or $1/\lambda^2$) at the free surface is

$$\lambda_r/\lambda_\theta = \bar{A}^2/(\bar{C}^2(1-{g_2}^2)+\bar{A}^2+{g_2}^2-1) \tag{21}$$

where $\bar{A} = A/B$ and $\bar{C} = C/B$. If the stretch ratio is set equal to the critical value ($\lambda_r/\lambda_\theta \approx 2.4$), the critical growth ratio for the formation of the surface creases in the inner layer is obtained

$${g_2}^2{}_{crit} = (\bar{C}^2+0.583\bar{A}^2-1)/(\bar{C}^2-1) \tag{22}$$

Similarly, we can have the critical growth ratio for interfacial crease formation

$${g_2}^2{}_{crit} = \alpha\bar{C}^2/(\alpha\bar{C}^2-\alpha+1) \tag{23}$$

where α is the critical stretch ratio for a given shear modulus ratio as shown in Fig. 5. Fig. 11 is a "phase diagram" showing the critical growth ratios for the onset of surface and interfacial creases with different initial geometries. The shear modulus ratio is set to $\mu_2/\mu_1 = 10$ which implies $\alpha = 3.23$ from Eq. (23). Based on the geometry and growth ratio of the outer layer, four highlighted regions can be determined. After growth, the structure could be in a flat state or develop surface creases and then form interfacial creases, or develop interfacial creases and then surface creases.

It is evident that, from Fig. 11, when the inner layer thickness is below ≈ 1.9 creasing always occurs in the free surface first, accompanied by interfacial creasing later. Another intriguing

observation is that an unusually high biological growth in a structure with a very thin outer layer is needed to trigger creases in the free surface while interfacial creases may happen earlier. It should be mentioned that all findings so far are related to the initiation of the creases based on the theoretical approach in which the growing bilayer structure is assumed to keep its axisymmetric pattern under any growth ratio. In the next section, non-linear finite element analysis will be performed to show the post-secondary morphological evolution after the system reaches the critical growth ratio predicted from the theoretical method.

D. Computational results

Fig. 12 shows the morphological evolution of a growing bilayer structure with $B = 1.4$. As discussed in Fig. 11, with the growth in the outer layer the stretch ratio in both layers grow and change the pattern of the structure. Fig. 12(a) shows the initial geometry of the model without growth. With growth in the outer layer, the structure starts to expand symmetrically (Fig. 12(b)) and after a certain value of growth ratio, the model loses its stability and develops surface creases first as shown in Fig. 12(c). With the continuation of growth, interfacial creases are observed at the interface of the two layers, as depicted in Fig. 12(d). Since the strain is identical at any place on the free surface under the axisymmetric deformation, any point on the free surface can attain the critical conditions necessary to start creasing. Therefore, the position and number of creases at the free surface cannot be perfectly determined by the critical condition for the initiation of creases, which is also valid for interfacial creases. However, pattern selection and the number of creases on the free surface or in the interfacial surface can be attributed to the process of minimizing the strain energy in the structure [18]. In Fig. 12, the free surface develops eight creases and with the continuation of growth they become deeper and sharper. After a certain amount of growth, four interfacial creases develop on the interface and then evolve into eight. This biological structure can continue to grow until the inner layer completely fills the free space of the structure.

Previous studies on the compressed flat bilayer structure show that beyond the critical strain ($\varepsilon_c = 0.35$) a flat surface develops creases with wavelength ω_{crease}:

$$\omega_{crease}/t \approx 3.5(1 -) \tag{24}$$

where t is the thickness of the film on the substrate before compression and is the compressive strain beyond the critical value [27,42]. By replacing with λ, Eq. (24) is represented by $\omega_{crease}/t = 3.5\lambda$. So, the wavelength of creases on the free surface can be calculated approximately and compared with numerical results. Eq. (24) is applicable when a uniform compressive strain is applied through the thickness of the film, whereas in the model of interest the strain and stretch through the thickness of inner layer is non-uniform as shown in Fig. 3. Compressive strain in the free surface of the inner layer is higher than the one at the interface. Since strain at the free surface is a more effective factor in determining the formation of surface creases, it can be estimated from Eq. (24). From Eq. (13) and with $g_2 = 1.2$, the stretch (λ) in the free surface can be determined as 0.320 which implies the dimensionless crease wavelength is $\omega_{crease}/t \approx 1.12$. From the computational model in Fig.12(c), this ratio is calculated as $\omega_{crease}/t \approx 1.10$. In the computational model the wavelength of creases is considered as a distance between two walls of a crease and measured from their middle line. The theoretical estimated value and computational result are in good agreement with each other, but it should be mentioned that the stretch (λ) from Eq. (13) is valid until the initiation of instability and after that critical point or at higher growth ratios it is no longer applicable. When the growth ratio increases, compressive strain builds up consequently in the inner layer and the wavelength of creases decreases as depicted in Fig. 12(e). Eq. (24) is just extracted for surface creases and cannot be used for the calculation of the interfacial crease wavelength. Depth of the creases is also a linear function of the applied compressive strain [27], a large strain corresponding to a deep crease as seen in Fig.12(e). It is intriguing to see that the sharp crease in the interfacial creases are formed towards the outer layer where the material is stiffer compared with the inner layer [30]. Our model proves that surface creases develop a self-contact pattern, but the presence of two materials in an interfacial crease prevents the interface from self-contact, therefore it forms a V-shape.

Fig. 13 shows the dynamic steps of morphological changes of a growing bilayer structure with different initial geometries. It can be implied that the thickness of the inner layer plays an important role in determining the creasing patterns of this biological structure. As expected from theoretical results and Fig. 11, the structure with a thin inner layer, e.g. $B = 1.1$, can

easily develop both surface and interfacial creases at almost the same time as shown in the bottom row of Fig. 13. The number of creases for both surface and interfacial creases is four. Before crease formation, the free surface deviates from the circular pattern which has not been predicted in the analytical approach. With the increase of the inner layer thickness, e.g. $B = 1.4$ or 1.7 surface creases come into the picture first followed by interfacial creases, which is consistent with the previous findings in Fig. 11. The number of creases is a function of both geometry and growth ratio. Competition between geometrical factors and growth ratios leads to the dynamic evolution of the number of creases in the structure which minimizes the strain energy of the growing structure. For the structure with a high thickness of the inner layer, e.g. $B = 1.9$, interfacial creases initially developed, followed by the free surface creases as shown in the top row of Fig. 13. At the beginning the number of interfacial creases is four, but with further growth more creases can be observed at the interface.

Critical growth ratios for the onset of both surface and interfacial creases extracted from FE analysis are compared with the theoretical findings in Fig. 11. Generally, there is a good agreement between theoretical and finite element results. Since the outer layer of the structure is stiffer than the inner layer, before crease formation the structure keeps symmetric in the FE analysis as the theoretical assumption states. This explains why good agreement is achieved between the theoretical and numerical results of the structure with a thin inner layer. For the structure with a thick inner layer, after a certain amount of growth the shape of its FE models deviates from circular. This deviation causes the discrepancy of the critical growth ratios between the theoretical value and the one from computational models.

Another factor which may affect the critical stretch ratio at the interface for creases is the shear modulus ratio between the two layers. Fig. 14 shows the morphological evolution of biological tubes with the same geometry but different shear modulus ratios. As expected from Fig. 10, the model with higher shear modulus ratio tends to develop interfacial creases earlier than the ones with lower shear modulus ratio. When the shear moduli of two layers are close to each other it is difficult to observe interfacial creases but there is evidence of a wrinkled pattern as shown in the bottom row of Fig. 14. Since the thickness ratio of the inner layer to the outer layer is the same for all three cases, the number of surface creases in all cases also remains the

same as evidenced in other papers [1,18]. But for interfacial creasing, the number of creases is also related to the shear modulus ratio. As expected, in Fig. 14 the number of interfacial creases is different for these three cases, and the model with a higher shear modulus ratio shows deeper and sharper creases than the model with a lower shear modulus does. For the ideal model with infinite shear modulus ratio, interfacial creases will be in a self-contact pattern as surface creases. Our results showed that when a soft layer grows on a stiffer layer, interfacial creases may be observed. As a proof to the results, a recent study in a flat bilayer structure with close stiffness of layers showed that when a soft layer grows on a substrate, at the first step and near the critical threshold the structure develops surface creases, while at a higher growth ratio and far from the threshold the structure develops interfacial creases while deepening surface creases [43]. Another experimental work backed by 3D numerical simulations for a multilayer cylindrical tube mimicking growth and villi formation of the gut also showed that growth in a constrained condition triggers instability and leads to the formation of different folding patterns [8]. A study to mimic the avascular development of thin solid tumors also showed that in a circular bilayer structure formed by the growth of the outer layer (ring) on a supporting core different kind of instabilities and patterns can be observed based on the stiffness ratio of the core to ring and thickness of the ring. With a high thickness of the growing ring and under special conditions interfacial wrinkles also were detected in the model [44]. Back to the bovine esophagi shown in Fig. 1, a muscle layer is much stiffer than the submucosal layer; after growth this causes interfacial creases are detected on the interface towards the muscle layer. As predicted and modeled, interfacial creases are usually growing into the stiffer materials. These findings show that mechanical parameters play a critical role in controlling surface patterns, although the development of these patterns are believed to be the consequence of the integrated and complex interactions among genetic, biochemical, and biological processes.

4. Conclusions

This paper explores surface and interfacial crease formation in a bilayer tubular biological tissue from an integrated theoretical and computational viewpoint. Both the stress distribution and the critical growth ratio for instability of the model and the formation of surface and interfacial

creases are determined. Results show that the initial geometry, growth ratio, and shear modulus ratio of the layers are the most determinant factors for tuning the starting point and patterns of surface or interfacial creases. Usually, a growing bilayer structure prefers to develop surface creases before interfacial creases. However in some special cases, for example with a very thin outer layer, interfacial creases can be observed to develop before surface creases. These findings can provide some fundamental understanding in the growth modeling of tubular biological tissues such as esophagi and airways, therefore offering useful insights into the diagnosis and prevention of pathological conditions.

No research, however, provides a perfect study; with this work being no exception to the rule. More endeavors should be devoted to expanding the realm of other types of instability in the tubular structure. For example, sometimes delamination phenomenon can be observed in layered biological tissues in the same manner as soft actuators or composite materials [45]. Also, besides biological soft tissues, the analytical and computational method presented here may be used as a tool to the quantification and calibration of soft multilayer artificial structures such as soft actuators in different environment conditions before and after the initiation of instability [46,47]. More endeavors should be devoted to exploring other various self-organized surface patterns in soft materials; these studies may open new windows towards advanced functional structure as an emerging technology [48], thereby leading to a simple but fundamental platform to design and measure the different surface instability in soft materials.

Acknowledgements

M.R. and X.W. acknowledge support from the University of Georgia (UGA) Startup Research Fund. R.P. appreciates the support from National Science Foundation with grant NO. 1430379.

References

[1] B. Li, Y.-P. Cao, X.-Q. Feng, and H. Gao, Soft Matter **8**, 5728 (2012).
[2] S. C. Cowin, Annu. Rev. Biomed. Eng. **6**, 77 (2004).
[3] W. Mönch and S. Herminghaus, Europhys. Lett. **53**, 525 (2001).

[4] S. Budday, P. Steinmann, and E. Kuhl, J. Mech. Phys. Solids. **72**, 75 (2014).
[5] A. M. Zöllner, A. Buganza Tepole, and E. Kuhl, J. Theor. Biol. **297**, 166 (2012).
[6] S. Budday, R. Nay, R. de Rooij, P. Steinmann, T. Wyrobek, T. C. Ovaert, and E. Kuhl, J. Mech. Behav. Biomed. Mater. **46**, 318 (2015).
[7] H.-C. Han, J. Biomech. **40**, 3672 (2007).
[8] A.E. Shyer, T. Tallinen, N.L. Nerurkar, Z. Wei, E.S. Gil, D.L. Kaplan, C.J. Tabin, L. Mahadevan, Science **342**, 212 (2013).
[9] B. Li, Y.-P. Cao, X.-Q. Feng, and H. Gao, J. Mech. Phys. Solids. **59**, 758 (2011).
[10] A. Guillou and R. W. Ogden, in Mechanics of Biological Tissue, edited by G. Holzapfel, and R. Ogden (Springer Berlin Heidelberg, 2006), pp. 47.
[11] D. Ambrosi and F. Mollica, Int. J. Eng. Sci. **40**, 1297 (2002).
[12] M. Ben Amar and A. Goriely, J. Mech. Phys. Solids. **53**, 2284 (2005).
[13] E. Kuhl, J. Mech. Behav. Biomed. Mater. **29**, 529 (2014).
[14] E. K. Rodriguez, A. Hoger, and A. D. McCulloch, J. Biomech. **27**, 455 (1994).
[15] C. Chuong and Y. Fung, in Frontiers in Biomechanics (Springer, 1986), pp. 117.
[16] J. Dervaux and M. B. Amar, Phys. Rev. Lett. **101**, 068101 (2008).
[17] G. Xu, P. V. Bayly, and L. A. Taber, Biomech. Model. Mechanobiol. **8**, 253 (2009).
[18] L. Jin, S. Cai, and Z. Suo, Europhys. Lett. **95**, 64002 (2011).
[19] M. J. Razavi and X. Wang, RSC Adv. **5**, 7440 (2015).
[20] T. Tallinen, J. S. Biggins, and L. Mahadevan, Phys. Rev. lett. **110**, 024302 (2013).
[21] E. Hohlfeld, L. Mahadevan, Phys. Rev. Lett. **109**, 025701(2012).
[22] T. Tallinen, J. S. Biggins, and L. Mahadevan, Phys. Rev. Lett. **110**, 024302 (2013).
[23] E. Hohlfeld and L. Mahadevan, Phys. Rev. Lett. **106**, 105702 (2011).
[24] L. Jin, A. Auguste, R.C. Hayward, Z. Suo, J. App. Mech. **82**, 061008 (2015).
[25] M. J. Razavi, T. Zhang, T. Liu, and X. Wang, Sci. Rep. **5**, 14477 (2015).
[26] T. Tallinen, J. Y. Chung, J. S. Biggins, and L. Mahadevan, Proc. Natl. Acad. Sci. **111**, 12667 (2014).
[27] Q. Wang and X. Zhao, Sci. Rep. **5**, 8887 (2015).
[28] S. Budday, E. Kuhl, J.W. Hutchinson, Philos. Mag. **95**, 3208 (2015).
[29] W. Hong, X. Zhao, and Z. Suo, Appl. Phys. Lett. **95**, 111901 (2009).
[30] L. Jin, D. Chen, R. C. Hayward, and Z. Suo, Soft Matter **10**, 303 (2014).
[31] Y.-P. Cao, B. Li, and X.-Q. Feng, Soft Matter **8**, 556 (2012).
[32] M. Eskandari, W. G. Kuschner, and E. Kuhl, Ann. Biomed. Eng. **43**, 2538 (2015).
[33] M. Eskandari, M. R. Pfaller, and E. Kuhl, Materials **6**, 5639 (2013).
[34] B. Li, F. Jia, Y.-P. Cao, X.-Q. Feng, and H. Gao, Phys. Rev. Lett. **106**, 234301 (2011).
[35] D. E. Moulton, A. Goriely, J. Mech.Phys. Solids. **59**, 525 (2011).
[36] A. Goriely, M. Robertson-Tessi, M. Tabor, and R. Vandiver, in Mathematical Modelling of Biosystems (Springer, 2008), pp. 1.
[37] Y. Cao, Y. Jiang, B. Li, and X. Feng, Acta. Mech. Solida Sin. **25**, 483 (2012).
[38] K. Brooks, M. J. Razavi, X. Wang, and J. Locklin, ACS nano **9**, 10961 (2015).

[39] M. J. Razavi, T. Zhang, X. Li, T. Liu, and X. Wang, Phys. Rev. E. **92**, 032701 (2015).
[40] Y. Cao and J. W. Hutchinson, J. appl. Mech. **79**, 031019 (2012).
[41] J.-Y. Sun, S. Xia, M.-W. Moon, K. H. Oh, and K.-S. Kim, Proc. R. Soc. A. **468**, 932 (2012).
[42] S. Cai, D. Chen, Z. Suo, and R. C. Hayward, Soft Matter **8**, 1301 (2012).

[43] T. Tallinen, John S. Biggins, Phys. Rev. E. **92**, 022720 (2015).

[44] J. Dervaux, M.B. Amar, J. Mech.Phys. Solids **59**, 538 (2011).

[45] E. Marinari, A. Mehonic, S. Curran, J. Gale, T. Duke, and B. Baum, Nature **484**, 542 (2012).
[46] Q. Wang, D. Robinson, and X. Zhao, Appl Phys Lett. **104**, 231605 (2014).
[47] B. Xu, D. Chen, and R. C. Hayward, Adv. Mater. **26**, 4381 (2014).
[48] Q. Wang and X. Zhao, MRS BULLETIN **41,** 115 (2016).

Figures

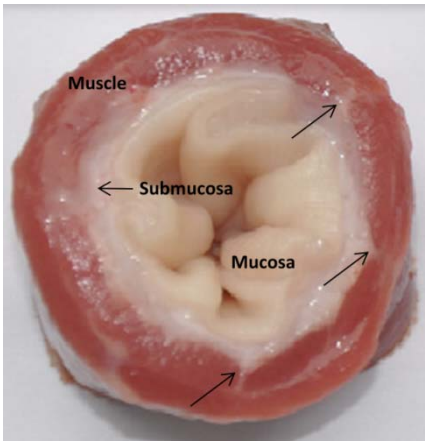

FIG. 1. Wrinkling of mucosa and interfacial creases in the esophagi of the bovine. Arrows show the sites of interfacial creases. Figure reprinted from Ref [9] with permission.

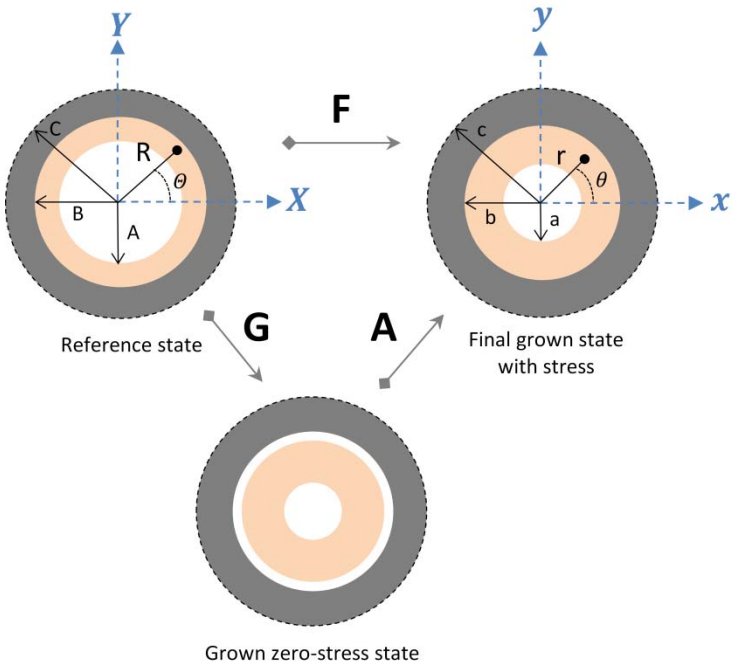

FIG. 2. Initial and current states of a growing structure. The deformation gradient (**F**) is decomposed into a growth tensor (**G**) and an elastic tensor (**A**).

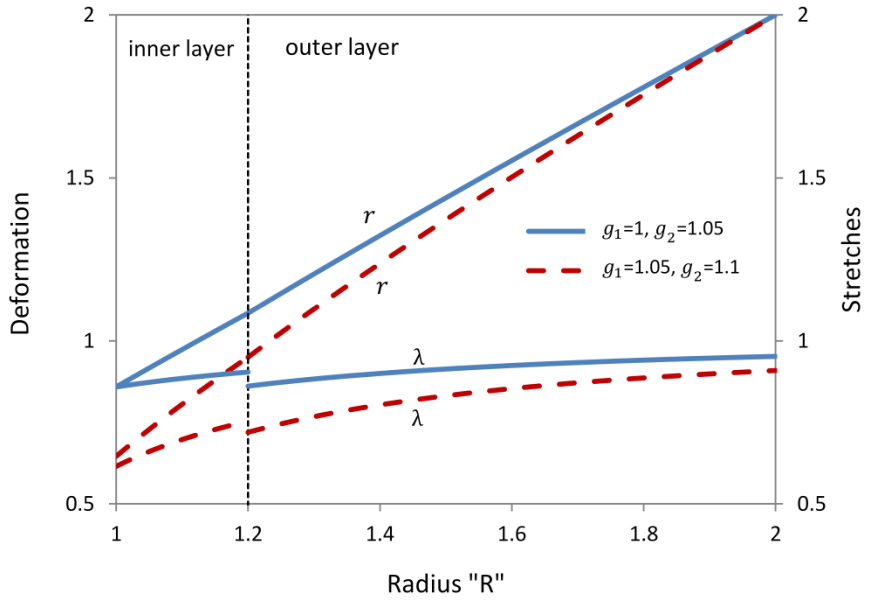

FIG. 3. Deformation field and stretches. $A = 1$, $C = 2$ and the interface is at B=1.2.

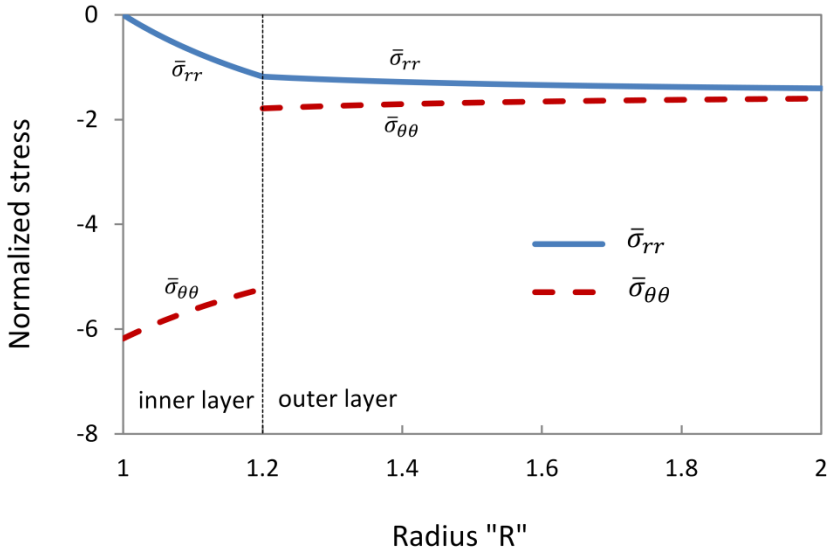

FIG. 4. Normalized radial and circumferential stresses in the growing structure. $A = 1$, $C = 2$ and the interface layer is at B=1.2. Growth only takes place in the outer layer, $g_2 = 1.05$.

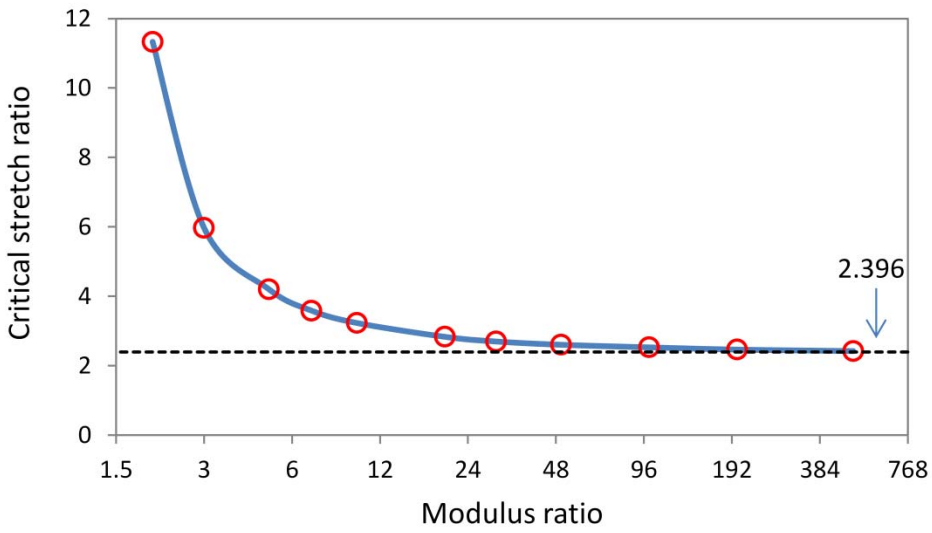

FIG. 5. The critical stretch ratio ($\lambda_r/\ \lambda_\theta$) for the onset of creases as a function of the shear modulus ratio, $\mu_2/\ \mu_1$. μ_2 is considered to be higher than μ_1.

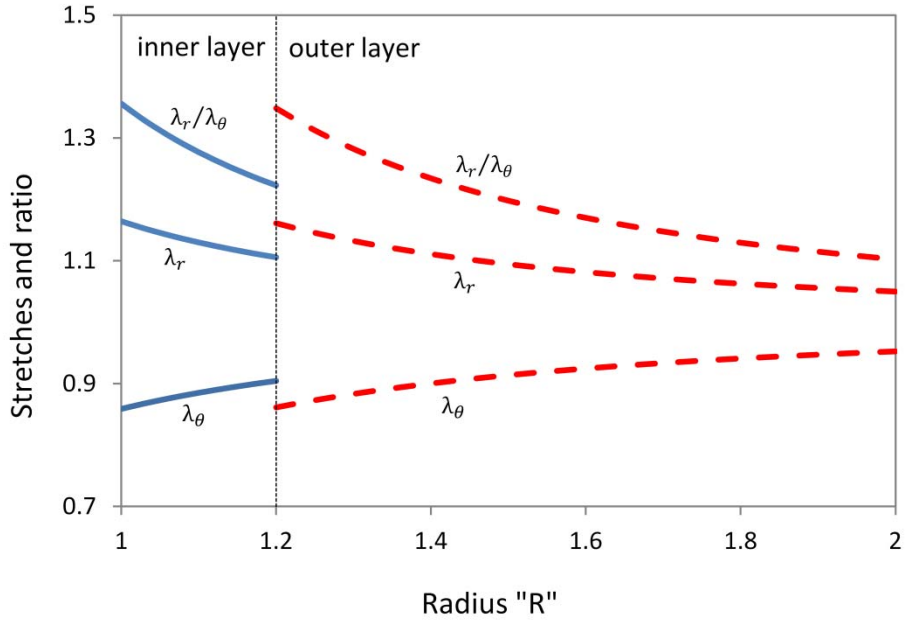

FIG. 6. Radial and circumferential stretches and their ratios for both inner and outer layer. $A = 1$, $C = 2$ and the interface layer is at B=1.2. Growth only takes place in the outer layer, $g_2 = 1.05$.

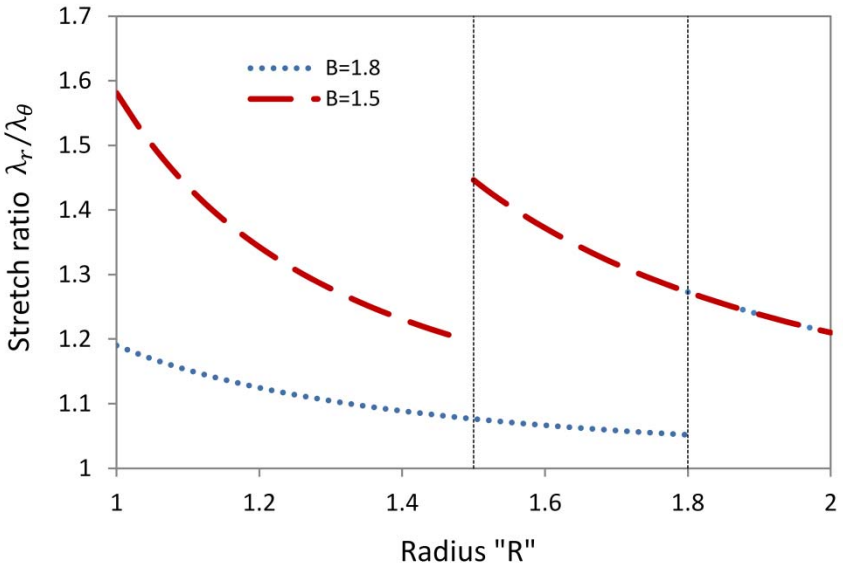

FIG. 7. Stretch ratios ($\lambda_r/\ \lambda_\theta$) for a growing structure with two different interfacial radii. $A = 1$, $C = 2$ and growth just takes place in the outer layer, $g_2 = 1.1$.

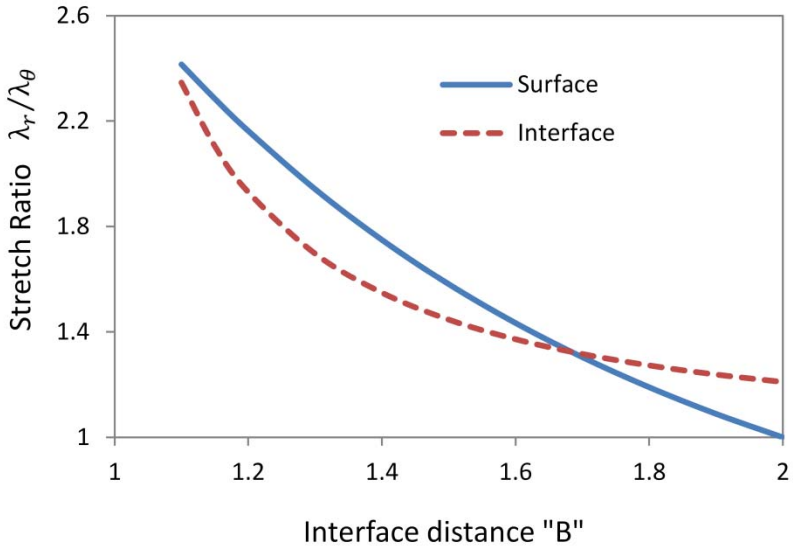

FIG. 8. Maximum stretch ratios at the free and interfacial surfaces. Growth only takes place in the outer layer, $g_2 = 1.1$ and $A = 1$, $C = 2$.

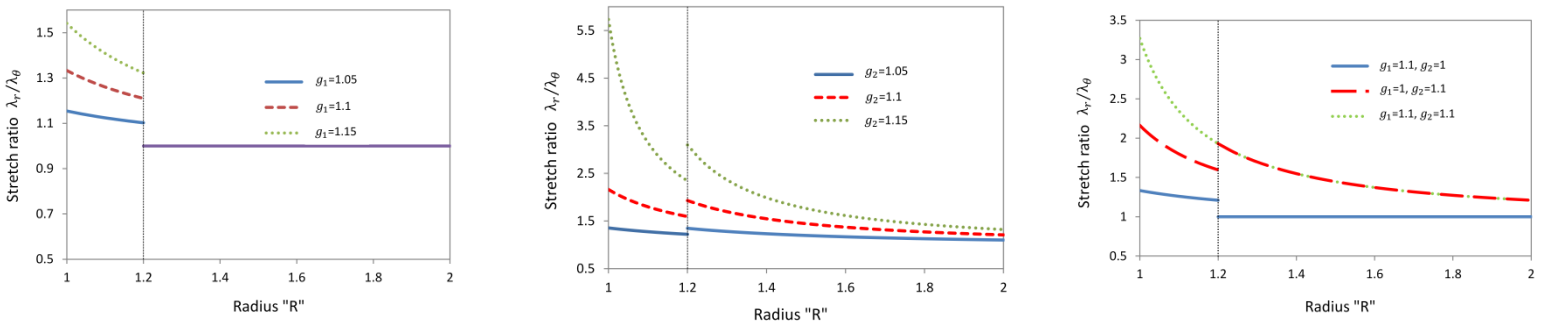

(a) (b) (c)

FIG. 9. Stretch ratios ($\lambda_r/\ \lambda_\theta$) for a structure with different growth ratios in the layers. (a) Growth only takes place in the inner layer; (b) growth only takes place in the outer layer; (c) growth takes place in both layers. For all cases $A = 1$, $B = 1.2$, and $C = 2$.

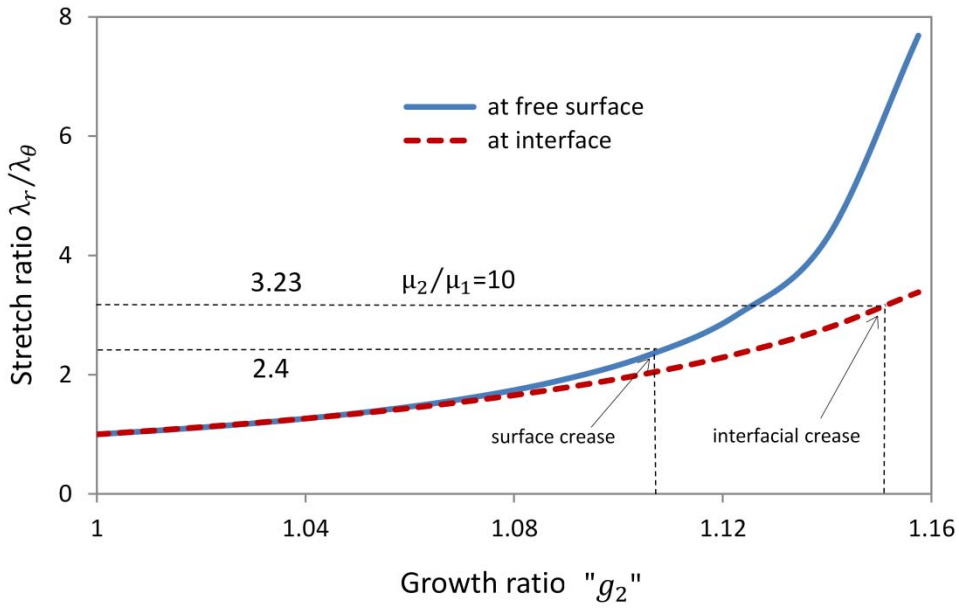

FIG. 10. Dependency of stretch ratios in the free and interfacial surfaces on the growth ratio. Growth only takes place in the outer layer. $A = 1$, $B = 1.2$, $C = 2$.

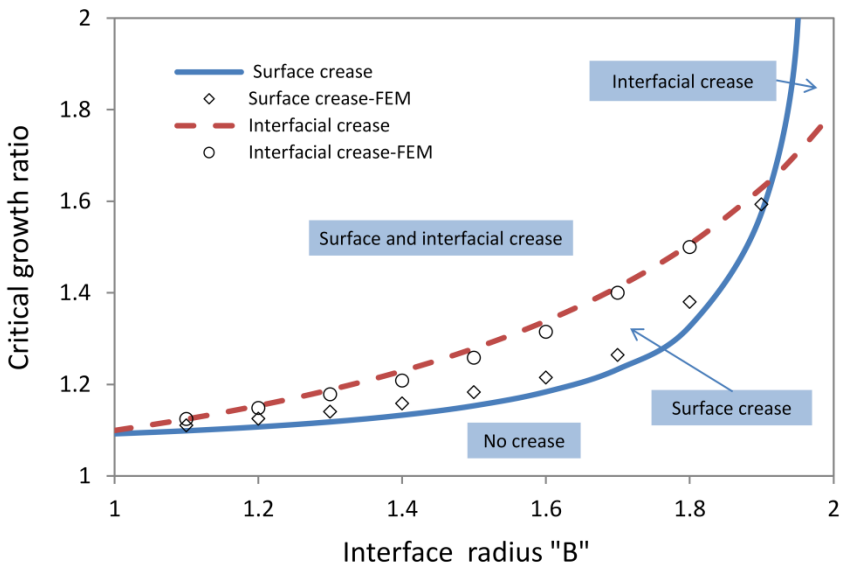

FIG. 11. Critical growth ratio for onset of surface and interfacial creases for the different inner layer thicknesses. Growth only takes place in the outer layer and $A = 1, C = 2, \mu_2/\mu_1 = 10$.

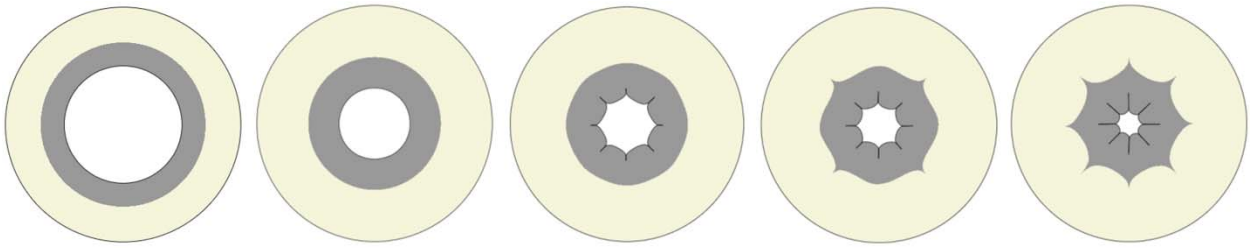

FIG. 12. (a)-(e); Step by step morphological evolution of a growing bilayer. Growth just takes place in the outer layer and $A = 1, B = 1.4, C = 2, \mu_2/\mu_1 = 10$.

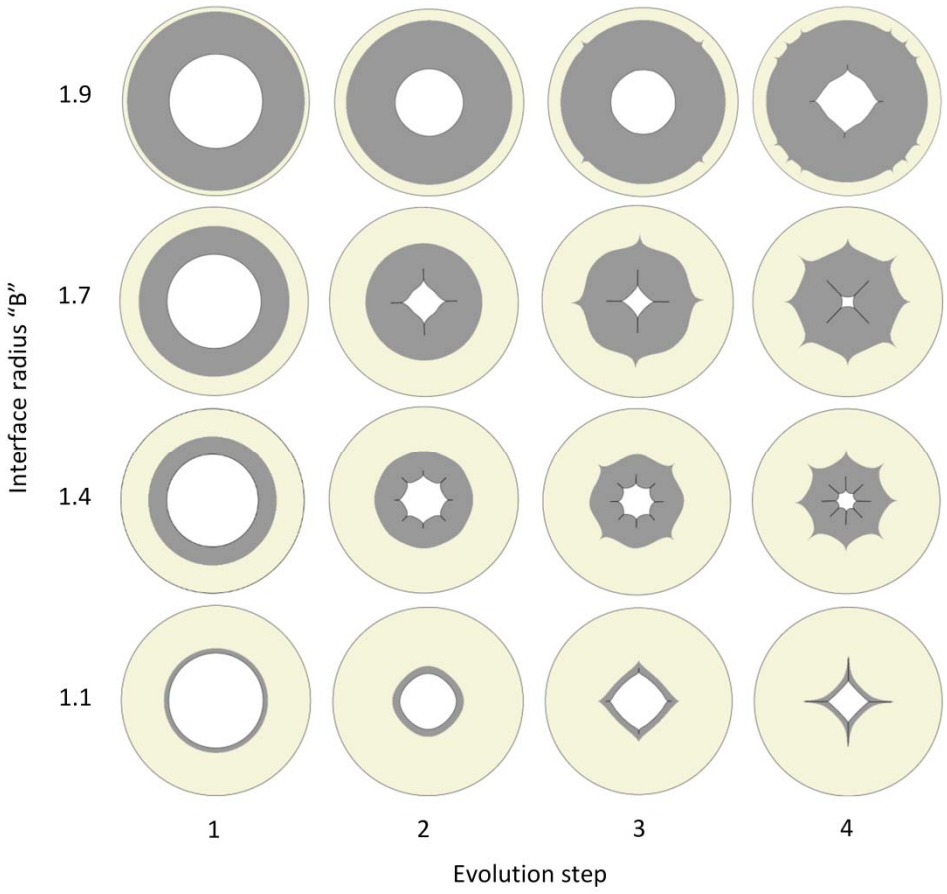

Fig. 13. Morphological evolution of a growing bilayer structure with different initial interface radiuses. Time step from 1 to 4 shows the evolution of morphology of the model (growth ratios are not same in columns). Growth only takes place in the outer layer and $A = 1, C = 2,\ \mu_2/\ \mu_1 = 10$.

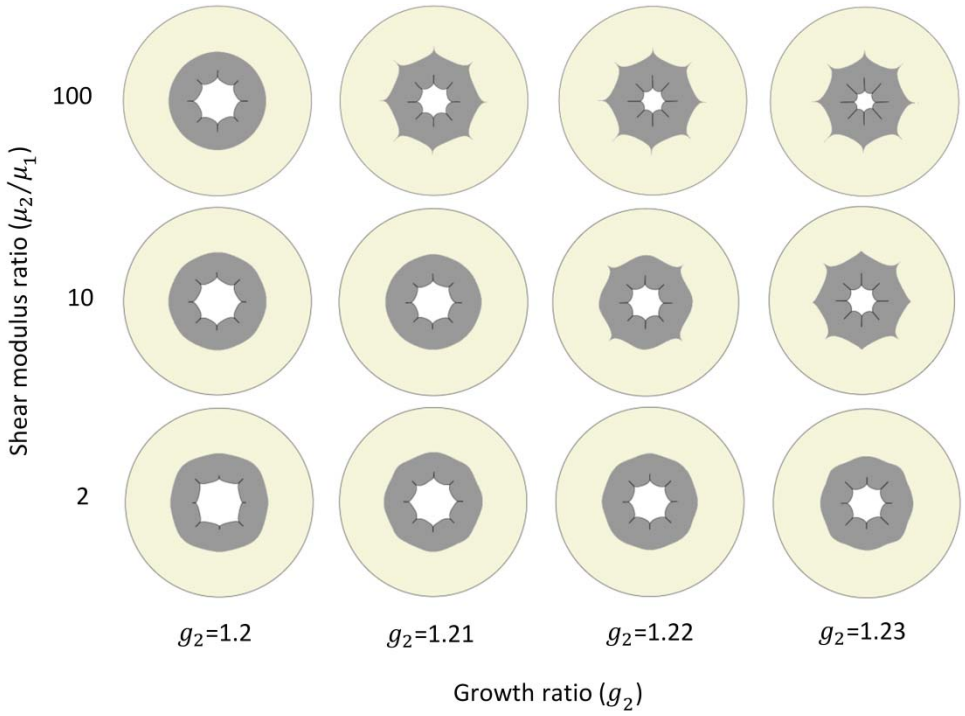

Fig. 14. Effect of the shear modulus ratio on the formation of interfacial creases. Growth only takes place in the outer layer and $\mathrm{A} = 1$, $B = 1.4$, $\mathrm{C} = 2$.